High-Frequency Rectifiers Based on Organic Thin-Film Transistors on Flexible Substrates

Ghada H. Ibrahim, Ute Zschieschang, Hagen Klauk, and Leonhard Reindl, *Senior Member, IEEE*

***Abstract*— Rectifier circuits featuring low threshold voltages and high cutoff frequencies based on p-channel organic thin-film transistors (TFTs) have been designed, fabricated and characterized. The TFTs and circuits were fabricated by shadow-mask lithography on flexible plastic substrates using the vacuum-deposited small-molecule organic semiconductor dinaphtho[2,3-b:2′,3′-f]thieno[3,2-b] thiophene (DNTT). The TFTs have a gate dielectric with a thickness of 5.3 nm and a channel length of 10 μm. The study considers the frequency characteristics of diode-connected transistors (transdiodes) and adopts circuit techniques from silicon CMOS technology, namely single-stage and multistage dynamic-threshold-compensated differential rectifiers. The characterization of the rectifier circuits indicates cutoff frequencies up to 4.75 MHz at a peak-to-peak input voltage of 3 V for transdiodes, up to 32 MHz at a peak-to-peak input voltage of 1.5 V for single-stage differential rectifiers and up to 7.5 MHz at a peak-to-peak input voltage of 1.5 V for two-stage rectifiers. The efficiency is 25% for a load of 10 MΩ and below 1% for a load of 1 MΩ.**

***Index Terms*— Organic thin-film transistors (TFTs), radio frequency identification (RFID), rectifier, transdiodes.**

I. Introduction

ORGANIC thin-film transistors (TFTs) are metal–insulator–semiconductor (MIS) field-effect-transistors in which the semiconductor is a thin layer of conjugated organic molecules [1]. Organic TFTs open many new opportunities for flexible electronics because they can be fabricated at low temperatures on plastic substrates with relatively simple fabrication processes, such as vapor or solution deposition [1]–[5].

One of the possible applications is in radio frequency identification (RFID) systems [6]. Traditionally, RFID tags are rigid devices, but many new application scenarios, such as wearable electronics, will benefit from the mechanical flexibility of the systems and hence, from the use of organic TFTs.

One of the circuit blocks comprising an RFID tag is the rectifier circuit that converts ac power received wirelessly by inductive or magnetic coupling into dc power required to operate the other parts of the system. An approach to implement these rectifier circuits is to use field-effect transistors operated in a diode-connected (transdiode) configuration, that is, with the gate electrode connected to the drain contact. The advantage of this approach is that it eliminates the need for diodes, which in thin-film electronics tend to be more difficult to fabricate than transistors [6]. An important consideration is that, unlike most of the other parts of the RFID system, the rectifier must be able to operate at the HF frequency, for example, at a standardized frequency of 13.56 MHz.

Benchmarking transdiode characteristics of TFTs usually focuses on their frequency response. For example, Semple *et al.* [7] reviewed the frequency characteristics of flexible TFTs and Schottky diodes fabricated using various organic semiconductors, metal oxides, and carbon nanomaterials. However, the frequency of operation was judged either by the cutoff frequency f_T and the maximum oscillation frequency f_{max} (in the case of TFTs based on metal oxides and carbon nanomaterials) or by the response at different frequency points (in the case of organic TFTs). Only a small number of publications have evaluated the frequency response of rectifier circuits based on transdiodes with threshold-voltage compensation. For example, Kawamura *et al.* [8] demonstrated dynamic-threshold-compensated rectifiers fabricated using inorganic metal–oxide TFTs that produced a dc output voltage of 12 V from an ac input voltage of ±18 V at a frequency of 13.56 MHz. Fiore *et al.* [9] reported a first-order threshold-compensated rectifier that delivered a dc output voltage of 25 V from a peak-to-peak ac input voltage of 60 V (±30 V) at a frequency of 13.56 MHz to a load of 0.7 MΩ.

We report here on the design and fabrication of single-stage and two-stage dynamic-threshold-compensated differential

Manuscript received January 9, 2020; revised March 16, 2020; accepted April 16, 2020. Date of publication May 12, 2020; date of current version May 21, 2020. This work was supported by the People Programme (Marie Curie Actions) of the European Union's Seventh Framework Programme through REA under Grant FP7/2007-2013 and Grant 609305 and in part by the German Research Foundation (DFG) under Grant KL 2223/6-1, Grant KL 2223/6-2 (SPP FFlexCom), and Grant KL 2223/7-1. The review of this article was arranged by Editor M. M. Hussain. *(Corresponding author: Ghada H. Ibrahim.)*

Ghada H. Ibrahim is with the Department of Microsystems Engineering, IMTEK, University of Freiburg, 79110 Freiburg im Breisgau, Germany, and also with the Electronics Research Institute, Giza 12622, Egypt (e-mail: ghada.abdelgawad@imtek.uni-freiburg.de).

Ute Zschieschang and Hagen Klauk are with the Max Planck Institute for Solid State Research, 70569 Stuttgart, Germany.

Leonhard Reindl is with the Department of Microsystems Engineering, IMTEK, University of Freiburg, 79110 Freiburg im Breisgau, Germany.

Color versions of one or more of the figures in this article are available online at http://ieeexplore.ieee.org.

Digital Object Identifier 10.1109/TED.2020.2989730

rectifiers based on p-channel organic TFTs fabricated on flexible plastic substrates and their characterization in terms of the frequency response under different loading conditions. The organic-TFT-based transdiodes showed cutoff frequencies up to 4.75 MHz at a peak-to-peak input voltage of 3 V, significantly above the TFTs' cutoff frequency predicted by common modeling approaches, while single-stage differential rectifiers showed a cutoff frequency of 32 MHz at an even lower peak-to-peak input voltage of 1.5 V. This bandwidth enhancement in organic-TFT-based differential rectifiers is a distinctive property not observed in silicon-FET-based differential rectifiers, since they are usually operated at frequencies below their theoretical frequency limits. The study reports a rigorous characterization of various organic-TFT-based rectifier circuits to provide a better understanding of the technology capabilities and proposed directions for nonquasistatic device modeling.

II. Fabrication

The organic TFTs were fabricated in the bottom-gate, top-contact (inverted staggered) device architecture on 125-μm-thick flexible polyethylene naphthalate substrates (Teonex Q65 PEN; kindly provided by William A. MacDonald, DuPont Teijin Films, Wilton, U.K.). In the first step of the fabrication process, 30-nm-thick gold was deposited onto the PEN substrate by thermal evaporation in vacuum through a polyimide shadow mask (CADiLAC Laser, Hilpoltstein, Germany) in order to define the interconnects and probe pads on the substrate surface. In the second step, a 30-nm-thick layer of aluminum was deposited through a second shadow mask to define the gate electrodes of the TFTs. The substrate was then briefly exposed to oxygen plasma to produce an aluminum oxide (AlO_x) layer with a thickness of 3.6 nm and then immersed into a 2-propanol solution of *n*-tetradecylphosphonic acid (PCI Synthesis, Newburyport, MA, USA) to allow a self-assembled monolayer (SAM) with a thickness of 1.7 nm to form on the plasma-oxidized aluminum surface. The resulting AlO_x/SAM gate dielectric thus has a total thickness of 5.3 nm and a unit-area capacitance of 700 nF/cm^2 [10]. In the third step, a 25-nm-thick layer of the small-molecule organic semiconductor dinaphtho[2,3-b:2′,3′-f]thieno[3,2-b]thiophene (DNTT; Sigma Aldrich) was deposited by sublimation in vacuum through a third shadow mask. During the DNTT deposition, the substrate was held at a temperature of 60 °C to induce a favorable thin-film morphology of the organic semiconductor layer. Finally, a 30-nm-thick layer of gold was deposited in vacuum through a fourth shadow mask to define the source and drain contacts. The TFTs have a channel length of 10 μm, gate-to-source and gate-to-drain overlaps of 30 μm each and channel widths ranging from 60 to 200 μm. Mask alignment was performed manually using an optical microscope. Except for the formation of the *n*-tetradecylphosphonic acid SAM that serves as part of the gate dielectric, this is an all-dry fabrication process that does not require photoresists, solvents, developers, or etchants. The TFTs are p-channel transistors and have an effective charge-carrier-mobility of 1 cm^2/Vs, a threshold voltage of -1 V, an ON-/OFF-current ratio of 10^8, and a subthreshold swing of 80 mV/decade. The TFTs' static performance parameters are summarized in Table I.

TABLE I
Device Parameters of the P-Channel Organic TFTs

Symbol	Definition	Value (unit)
L	Channel length	10 (μm)
L_{ov}	Gate-drain/gate-source overlap	30 (μm)
$I_{ON/OFF}$	On/Off current ratio	10^8
$S_{S\text{-}TH}$	Subthreshold swing	80 (mV/dec)
μ_{eff}	Effective mobility	1.0 (cm^2/Vs)
V_{th}	Threshold voltage	-1.0 (V)
C_{diel}	Insulator capacitance per unit area	700 (nF/cm^2)

III. Modeling

Modeling of the static and dynamic characteristics of organic TFTs has gained considerable interest. Successful modeling provides two important benefits: A better understanding of the electrical behavior of the TFTs and a platform for the design of circuits with higher complexity. A complete model would be able to accurately describe the linear/nonlinear, dc/ac, quasistatic/nonquasistatic, and small-signal/large-signal behavior of the devices. Well-established organic-TFT models are the dc models [11]–[13], the small-signal models that incorporate device parasitics in the quasistatic regime [14], and combined dc/ac models [15], [16]. Large-signal nonquasistatic operation, on the other hand, has so far rarely been addressed [17].

To characterize the rectifying properties of organic-TFT-based transdiodes, the maximum frequency of operation is one of the parameters that needs to be evaluated. Earlier frequency-response modeling efforts for organic TFTs [1], [18] reported a small-signal current-gain cutoff frequency given by

$$f_{\mathrm{T}} = \frac{\mu_{\mathrm{eff}}(V_{\mathrm{GS}} - V_{\mathrm{th}})}{2\pi L\left(\frac{2}{3}L + 2L_{\mathrm{ov}}\right)} \tag{1}$$

where μ_{eff} is the effective mobility, V_{th} is the threshold voltage, L is the channel length, and L_{ov} is the gate-to-source and gate-to-drain overlap length.

Another important dynamic-performance parameter is the effective delay of gate-induced charges, τ, which indicates the time required to induce the charges in the channel and which is given by

$$\tau = \frac{R_{\mathrm{sheet}} C_{\mathrm{diel}} L^2}{2} \tag{2}$$

where R_{sheet} is the sheet resistance of the charge-carrier channel and C_{diel} is the gate-dielectric capacitance per unit area. It is important to note that these device parameters were extracted in [1] by admittance characterization methods under small ac excitation of $\pm$100 mV.

As transdiodes are excited by large ac signals and target frequencies are well above their quasistatic operating regime, f_{T} and τ may not be real measures of the highest achievable operating frequencies of transdiodes. Although transdiodes

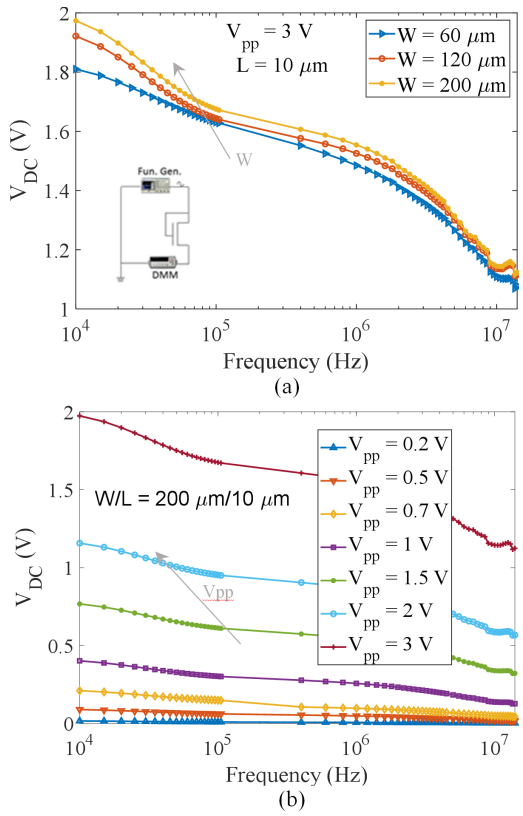

Fig. 1. Transdiode characterization results. (a) DC output voltage measured for a sinusoidal input voltage with an amplitude (V_{pp}) of 3 V and frequencies ranging from 10 kHz to 14 MHz. Results are shown for transdiodes based on organic TFTs with a channel length of 10 μm and channel widths of 60, 120, and 200 μm. The inset shows the measurement setup. (b) DC output voltage measured for sinusoidal input voltages with amplitudes ranging from 0.2 to 3.0 V for a transdiode based on a TFT with a channel length of 10 μm and a channel width of 200 μm. The output load impedance is 10 M Ω.

have not yet received a careful physical modeling approach, Uno *et al.* [19] derived a theoretical maximum frequency f_{max} given by

$$f_{max} = \frac{\mu}{2L^2} V_0 \left(\frac{\sqrt{1-\beta^2}}{\cos^{-1}\beta} - \beta \right) \tag{3}$$

where V_0 is the amplitude of the ac input voltage and $\beta = (V_{OUT}/V_0)$. Equation (3) was derived under the assumption that a transdiode can be modeled as an *RC* circuit that charges an output node to an output voltage V_{OUT} when the device is in the ON-state and in the saturation regime [19]. The theoretical maximum frequency f_{max} is said to be π times higher than the transit frequency f_T of the transistor.

In Section VI, the above-mentioned frequency parameters f_T, τ, and f_{max} will be revisited and examined in terms of their suitability for describing and benchmarking the operational frequency limits of the rectifier circuits presented below.

IV. Transdiode Characterization

To evaluate the rectification properties of organic-TFT-based transdiodes, we measured several devices using a computer-controlled measurement setup with a multicontact probe.

All measurements were performed under ambient conditions. Transdiodes based on organic TFTs with channel lengths (L) of 10 μm and channel widths (W) of 60, 120, and 200 μm were characterized. The results are summarized in Fig. 1. Fig. 1(a) shows the dc output voltage (V_{dc}) measured for a sinusoidal input voltage with an amplitude (peak-to-peak voltage V_{pp}) of 3 V and frequencies ranging from 10 kHz to 14 MHz. Fig. 1(b) shows the dc output voltage measured for sinusoidal input voltages with amplitudes (V_{pp}) ranging from 0.2 to 3.0 V and frequencies ranging from 10 kHz to 14 MHz for a transdiode based on a TFT with a channel length of 10 μm and a channel width of 200 μm.

It can be seen that the magnitude of the dc output voltage increases with increasing channel width, that is, with increasing transconductance of the TFT. If we define the cutoff frequency of the rectifier circuit as the frequency at which the rectified voltage is smaller by a factor of $\sqrt{2}$ than its maximum (low-frequency) value, as in [19], we estimate a cutoff frequency of about 4.75 MHz at an amplitude (V_{pp}) of 3 V. The open-circuit output voltage measured at a frequency of 13.56 MHz is 1.1 V.

V. Rectifier Circuit Design and Characterization

To compensate for the higher threshold voltage of transdiode-based rectifiers compared with diode-based rectifiers, either static or dynamic threshold-voltage (V_{th}) compensation must be implemented. In static threshold-voltage compensation, the compensation voltage is constant and independent of the applied ac input voltage. Static threshold-voltage compensation leads to smaller ON-state resistance but larger OFF-state leakage currents. Dynamic threshold-voltage compensation employs a cross-coupled differential-circuit configuration that increases the forward bias voltage on the device in the ON-state, as well as the reverse bias voltage in the OFF-state. This emulates a reduction of V_{th} in the ON-state and an increase of V_{th} in the OFF-state, denoted in [20] as "active" V_{th} cancellation.

The circuit diagram of the dynamic-threshold-voltage-compensated differential drive is shown in Fig. 2(a), while the photograph of the fabricated circuit is shown in Fig. 2(b) and the measurement setup is illustrated in Fig. 2(c). The TFTs M1-M4 have a channel length (L) of 10 μm and the same channel width (W). The coupling capacitors (C_C) have an area of $W \times W$. Circuits based on TFTs with channel widths of 60, 120, and 200 μm were fabricated and characterized. M3 and M4 are diode-connected TFTs, while M1 and M2 are switch-connected so that the gate–source and drain–source voltages alternatively and interchangeably attain maximum positive and negative values, which leads to maximum overdrive in the forward condition and minimum overdrive in the reverse condition [20], [21]. The influence of the coupling capacitance, also referred to as pumping capacitance, was quantitatively studied by Mandal and Sarpeshkar [22] who also showed that it is beneficial to scale the coupling capacitance proportionally with the transconductance of the transistors.

As the coupling capacitors form part of a capacitive voltage divider controlling the voltage applied to the gate electrodes of

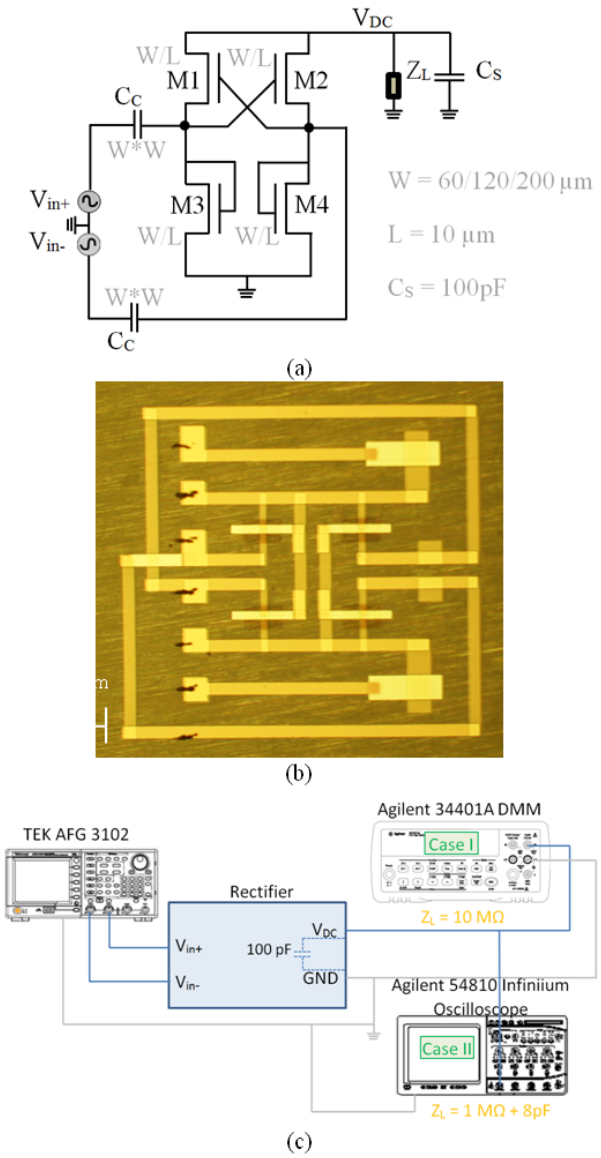

Fig. 2. Single-stage differential-drive dynamic-threshold-voltage-compensated rectifier. (a) Circuit diagram. (b) Photograph (3 mm × 2.8 mm). (c) Measurement setup.

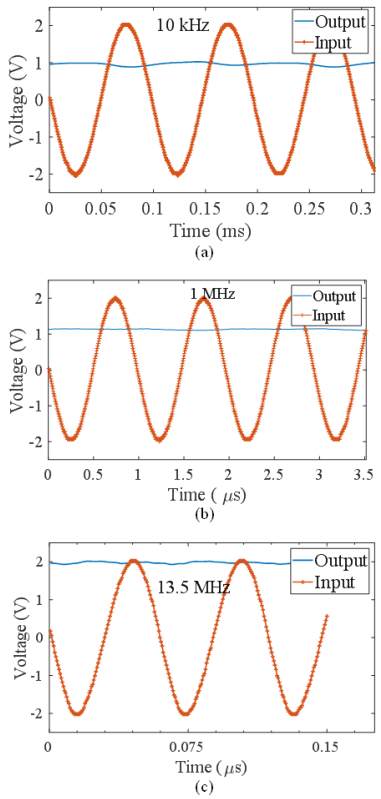

Fig. 3. Single-stage differential-drive dynamic-threshold-voltage-compensated rectifier characterization results. Output voltage measured at input sinusoidal frequencies of (a) 10 kHz, (b) 1 MHz, and (c) 13.5 MHz.

the transistors, larger capacitances were implemented in order to compensate for the influence of the overlap capacitances of the TFTs [1]. On the other hand, the circuit layout was optimized to avoid interconnect crossings and the parasitic capacitances associated with them (≈about 1 μF/cm^2, [1]). The only crossing was designed intentionally at the output nodes in order to create a smoothing capacitor with a capacitance of about 100 pF, denoted as C_s in Fig. 2(a).

Two test setups were used, as shown in Fig. 2(c). A Tektronix 3102 signal generator was used in both cases for generating two differential sinusoidal signals as the rectifier ac input. An Agilent 34401A digital multimeter was used to measure the rectified dc output voltage over a wide range of input frequencies [denoted as case I in Fig. 2(c)]. Time-domain measurements were performed using an Agilent Infiniium 54810 oscilloscope in order to obtain accurate ac information, including ripple. Results of time-domain measurements performed with sinusoidal input signals with frequencies of 10 kHz, 1, and 13.5 MHz are shown in Fig. 3. In all cases, the rectifier produces a steady dc voltage with a relatively small ripple of about 150 mV at a frequency of 10 kHz, 53 mV at a frequency of 1 MHz and 86 mV at a frequency of 13.56 MHz.

Although the performance of the differential-drive dynamic-threshold-compensated rectifier shown in Fig. 2(a) is predicted to be similar to that of full-wave dynamic-threshold-compensated rectifiers [23], our characterization results show different trends in terms of frequency response and dependence on the channel width of the transistors. Fig. 4(a) shows the results of measurements performed on the rectifier circuit shown in Fig. 2, based on TFTs with a channel length (L) of 10 μm and channel widths (W) of 60, 120, and 200 μm. Two important observations are made: First, the dc output voltage increases with decreasing channel width of the TFTs. This can be explained by the fact that a dynamically threshold-voltage-compensated rectifier contains switches and that the larger parasitic capacitances, and larger leakage currents resulting from the larger channel width are more detrimental to the rectification behavior in this case than the smaller ON-state resistance. This means that the optimum transistor size is smaller in the rectifier circuit proposed here.

Although analytical methods have been derived previously for rectifiers based on silicon MOSFETs in order to predict the optimum transistor size based on quasistatic transistor models [23], it is not currently possible to use the same

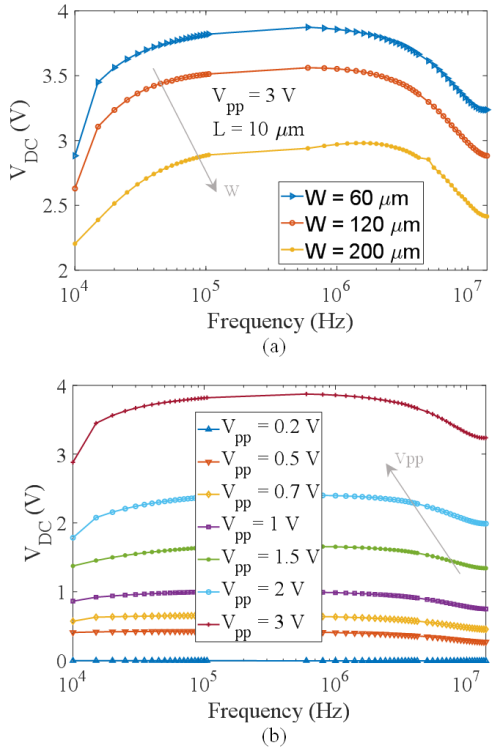

Fig. 4. Single-stage differential-drive dynamic-threshold-voltage-compensated rectifier characterization results. (a) DC output voltage measured for a sinusoidal input voltage with an amplitude of 3 V for channel widths of the transistors M1–M4 of 60, 120, and 200 μm. (b) DC output voltage measured for a sinusoidal input voltage with an amplitude ranging from 0.2 to 3.0 V for a channel width of the transistors of 60 μm. All TFTs have a channel length of 10 μm. The output load impedance is about 10 MΩ.

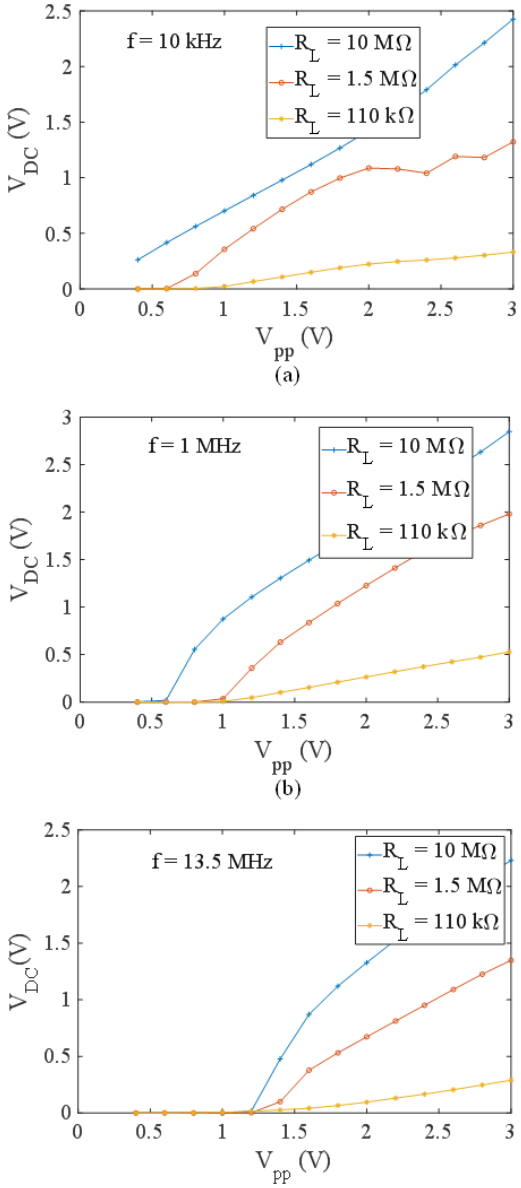

Fig. 5. DC output voltage of a single-stage differential-drive dynamic-threshold-voltage-compensated rectifier measured with output-load impedances of 110 kΩ, 1.5 MΩ, and 10 MΩ for a sinusoidal input voltage with amplitudes ranging from 0.2 to 3 V and frequencies of (a) 10 kHz, (b) 1 MHz, and (c) 13.5 MHz.

analytical approach here, as we are operating the organic TFTs far beyond their theoretical cutoff frequency in the nonquasistatic regime, which is a mode of operation that has not been reliably modeled so far.

The second observation is that the dynamic-threshold-voltage-compensated rectifier shows bandpass behavior: At low frequencies, the dc output voltage is limited by the coupling capacitance, while at high frequencies, it is limited by the transit frequency of the transistors. The cutoff frequency is notably larger than that of the transdiodes in Fig. 1. Fig. 4 shows that at a frequency of 13.56 MHz, an open-circuit dc output voltage of 3.24 V can be extracted from an ac input voltage with an amplitude of 3 V. A cutoff frequency of 32 MHz is estimated for the rectifier cells based on TFTs with a smallest channel width of 60 μm.

While Fig. 4(a) and (b) shows the dc output voltage measured using a digital multimeter with a high-impedance load of about 10 MΩ, Fig. 5 shows the dc output voltage measured with load impedances of 110 kΩ, 1.5 MΩ, and 10 MΩ under different loading conditions and at different frequencies.

The rectifier efficiency reaches a maximum of 25% at a frequency of 20 kHz for a load of 10 MΩ with an output power of 0.3 μW. The efficiency is above 20% for frequencies ranging from 20 to 200 kHz and a load of 10 MΩ. When the load is smaller than 1 MΩ, the efficiency drops below 1% with a maximum output power of 2 μW in the frequency range from 20 kHz to 2 MHz. Fig. 6 shows the efficiencies measured for a rectifier circuit based on TFTs with a channel length of 10 μm and a channel width of 120 μm.

By connecting two dynamic-threshold-voltage-compensated rectifier cells in series, output-voltage doubling can be achieved. Fig. 7 shows a photograph and the dc output voltage of a two-stage dynamic-threshold-voltage-compensated rectifier measured for a sinusoidal input voltage with amplitudes ranging from 0.2 to 1.5 V and frequencies ranging from 10 kHz to 13.56 MHz. The cutoff frequency of this circuit is estimated to be 7.5 MHz, that is, less than that of the single-stage rectifier in Fig. 4 due to larger capacitive loading.

A comparison of the performance characteristics of the transdiode and the single-stage differential (cross-coupled)

TABLE II
COMPARISON OF DIFFERENT ORGANIC RECTIFIERS

	This work		[24]	[9]	[25]		[26]
Architecture	Transdiode	Cross-coupled rectifier	Vertical diode	1st order V_{th} Comp. Rect.	Transdiode	Cross-coupled rectifier	Vertical diode
Load impedance (R, C)	10 MΩ, 113 pF	1.5 MΩ, 113pF	1 MΩ	0.7 MΩ	22 MΩ, 1 µF	22 MΩ, 1 µF	1 MΩ, 100 nF
13.5 MHz (V_{out}/V_{ac})	1.1 V / 3 V	1.4 V / 3 V	3.5 V / 10 V	25 V / 30 V	2.65 V/ 10 V (at 1 kHz)	3.3 V / 10 V (at 1 kHz)	6.66 V / 10 V
Cutoff frequency	4.75 MHz	32 MHz (at 10 MΩ)	≈ 7 MHz	-	-	-	85.7 MHz after annealing

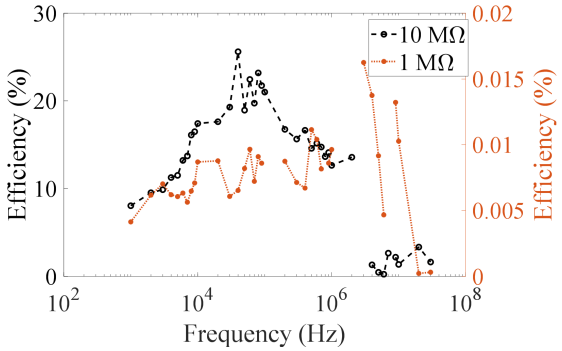

Fig. 6. Efficiency of a single-stage differential-drive dynamic-threshold-voltage-compensated rectifier based on organic TFTs with a channel length of 10 μm and a channel width of 120 μm for an output-load impedance of 10 MΩ (left axis) and 1 MΩ (right axis).

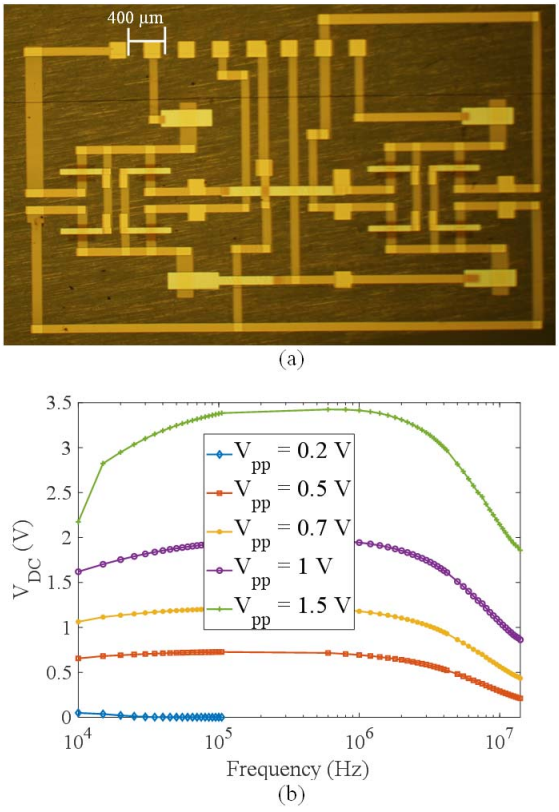

Fig. 7. (a) Photograph (6 mm × 3,7 mm) and (b) dc output voltage of a two-stage differential-threshold-voltage-compensated rectifier based on organic TFTs with a channel length of 10 μm and a channel width of 120 μm measured for a sinusoidal input voltage with amplitudes ranging from 0.2 to 1.5 V and frequencies ranging from 10 kHz to 13.56 MHz.

rectifier presented here with those of rectifiers based on organic TFTs reported in the literature is presented in Table II.

VI. Discussion and Conclusion

In order to assess how the cutoff frequencies estimated from the measured frequency response of the rectifier circuits in Sections IV and V compare to the theoretically predicted cut-off frequencies derived in Section III, we have used (1) and (2) to calculate the cutoff frequency and the transit time of the transistors employed in the rectifier circuits. The TFTs have a gate-dielectric capacitance (C_{diel}) of 700 nF/cm^2, a channel length (L) of 10 μm, gate-to-source and gate-to-drain overlaps (L_{ov}) of 30 μm each, an effective charge-carrier mobility (μ_{eff}) of 1 cm^2/Vs, and a threshold voltage of -1 V. The cutoff frequency f_T calculated using (1) for a gate–source voltage (V_{GS}) of -3 V is about 50 kHz. This cutoff frequency is limited mainly by the gate-to-contact overlaps; without overlaps ($L_{ov} = 0$), (1) would yield a cutoff frequency close to 500 kHz. The transit time τ calculated using (2) for a sheet resistance (R_{sheet}) of 500 kΩ/sq is 175 ns, which implies that carrier-channel formation and annihilation can be induced at frequencies up to about 5 MHz. In other words, the inverse of the transit time ($1/\tau$) calculated using (2) is two orders of magnitude larger than the cutoff frequency f_T calculated using (1), but only one order of magnitude larger than f_T calculated in the absence of gate-to-contact overlaps (similar to [19]). The maximum frequency f_{max} calculated using (3) is 140 kHz, that is, about a factor of three larger than the cutoff frequency f_T calculated using (1), but a factor of 30 smaller than the inverse of the transit time ($1/\tau$) calculated using (2).

From the measurements on our transdiodes, we estimate a cutoff frequency of 4.75 MHz at a peak-to-peak input voltage of 3 V. This estimate exceeds the cutoff frequency f_T calculated using (1) by almost two orders of magnitude and the maximum frequency f_{max} calculated using (3) by more than one order of magnitude, but it is in good agreement with the transit time τ calculated using (2).

We thus conclude that the transit time τ calculated using (2) provides a more realistic limit for the maximum operating frequency of transdiode rectifiers, which suggests that the latter is limited by the formation and annihilation of the charge-carrier channel in the semiconductor, rather than by the device capacitance. This can be attributed to the fact that in the transdiode configuration, the transistor is operated as a passive device without providing gain, whereas the cutoff frequency f_T calculated using (1) is a measure of the ability of the transistor to provide gain.

The cutoff frequency estimated for the single-stage dynamic-threshold-voltage-compensated rectifiers is even higher, 32 MHz. This is related to the bandpass behavior of the circuits, as a result of which the dc output voltage reaches its

maximum at a relatively high frequency (about 1 MHz in our case), so that a very high cutoff frequency is estimated when the usual definition for the cutoff frequency is applied [19].

To conclude, we have experimentally evaluated the frequency characteristics of transdiodes as well as single-stage and two-stage dynamic-threshold-voltage-compensated rectifier circuits based on organic TFTs fabricated on flexible plastic substrates. We have shown that the dynamic-threshold-voltage-compensated rectifiers show an improved frequency response compared to transdiodes, which is a property that is not usually observed in rectifiers based on silicon MOSFETs. A possible explanation is that the operation of silicon-MOSFET-based rectifiers is usually reported only for the quasistatic domain, not for nonquasistatic operation. This implies that the design of such circuits in the future will benefit greatly from more accurate modeling of the nonquasistatic operation of organic TFTs.

The high-frequency operation of the differential rectifiers reported here not only suggests the feasibility of organic-TFT-based RFID systems but also opens up various possibilities of designing wearable wireless power-transfer systems to power medical sensors, making use of the mechanical flexibility of circuits based on organic TFTs and of printed antennas.

ACKNOWLEDGMENT

Ghada H. Ibrahim would like to thank Prof. Yiannos Manoli for providing the infrastructure for the design and measurement.

REFERENCES

[1] T. Zaki, *Short-channel Organic Thin-film Transistors: Fabrication, Characterization, Modeling and Circuit Demonstration*. Cham, Switzerland: Springer, 2015.

[2] D. M. Taylor, "Vacuum-thermal-evaporation: The route for roll-to-roll production of large-area organic electronic circuits," *Semicond. Sci. Technol.*, vol. 30, no. 5, May 2015, Art. no. 054002, doi: 10.1088/0268-1242/30/5/054002.

[3] T. Zaki *et al.*, "A 3.3 v 6-Bit 100 kS/s current-steering digital-to-analog converter using organic P-type thin-film transistors on glass," *IEEE J. Solid-State Circuits*, vol. 47, no. 1, pp. 292–300, Jan. 2012, doi: 10.1109/JSSC.2011.2170639.

[4] G. Giri *et al.*, "Tuning charge transport in solution-sheared organic semiconductors using lattice strain," *Nature*, vol. 480, no. 7378, pp. 504–508, Dec. 2011, doi: 10.1038/nature10683.

[5] J. W. Borchert *et al.*, "Small contact resistance and high-frequency operation of flexible low-voltage inverted coplanar organic transistors," *Nature Commun.*, vol. 10, no. 1, p. 1119, Dec. 2019, doi: 10.1038/s41467-019-09119-8.

[6] S. Steudel *et al.*, "50 MHz rectifier based on an organic diode," *Nature Mater.*, vol. 4, pp. 597–600, Jul. 2005, doi: 10.1038/nature10683.

[7] J. Semple, D. G. Georgiadou, G. Wyatt-Moon, G. Gelinck, and T. D. Anthopoulos, "Flexible diodes for radio frequency (RF) electronics: A materials perspective," *Semiconductor Sci. Technol.*, vol. 32, no. 12, Dec. 2017, Art. no. 123002, doi: 10.1088/1361-6641/aa89ce.

[8] T. Kawamura *et al.*, "Oxide TFT rectifier achieving 13.56-MHz wireless operation with DC output up to 12 V," in *IEDM Tech. Dig.*, San Francisco, CA, USA, Dec. 2010, pp. 21.4.1–21.4.4, doi: 10.1109/IEDM.2010.5703407.

[9] V. Fiore *et al.*, "An integrated 13.56-MHz RFID tag in a printed organic complementary TFT technology on flexible substrate," *IEEE Trans. Circuits Syst. I, Reg. Papers*, vol. 62, no. 6, pp. 1668–1677, Jun. 2015, doi: 10.1109/TCSI.2015.2415175.

[10] U. Zschieschang and H. Klauk, "Low-voltage organic transistors with steep subthreshold slope fabricated on commercially available paper," *Organic Electron.*, vol. 25, pp. 340–344, Oct. 2015, doi: 10.1016/j.orgel.2015.06.038.

[11] O. Marinov, M. J. Deen, U. Zschieschang, and H. Klauk, "Organic thin-film transistors: Part I—Compact DC modeling," *IEEE Trans. Electron Devices*, vol. 56, no. 12, pp. 2952–2961, Dec. 2009, doi: 10.1109/TED.2009.2033308.

[12] M. J. Deen, O. Marinov, U. Zschieschang, and H. Klauk, "Organic thin-film transistors: Part II—Parameter extraction," *IEEE Trans. Electron Devices*, vol. 56, no. 12, pp. 2962–2968, Dec. 2009, doi: 10.1109/TED.2009.2033309.

[13] L. Colalongo, "SQM-OTFT: A compact model of organic thin-film transistors based on the symmetric quadrature of the accumulation charge considering both deep and tail states," *Organic Electron.*, vol. 32, pp. 70–77, May 2016, doi: 10.1016/j.orgel.2016.02.005.

[14] O. Marinov and M. J. Deen, "Quasistatic compact modelling of organic thin-film transistors," *Organic Electron.*, vol. 14, no. 1, pp. 295–311, Jan. 2013, doi: 10.1016/j.orgel.2012.10.031.

[15] M. Fadlallah, G. Billiot, W. Eccleston, and D. Barclay, "DC/AC unified OTFT compact modeling and circuit design for RFID applications," *Solid-State Electron.*, vol. 51, no. 7, pp. 1047–1051, Jul. 2007, doi: 10.1016/j.sse.2007.05.018.

[16] L. Jiang, E. Ei-Masry, and I. G. Hill, "Static and dynamic modeling of organic thin-film transistors for circuit design," *Microelectron. J.*, vol. 53, pp. 1–7, Jul. 2016, doi: 10.1016/j.mejo.2016.04.012.

[17] A. Valletta, M. Rapisarda, S. Calvi, L. Mariucci, and G. Fortunato, "A large signal non quasi static model of printed organic TFTs and simulation of CMOS circuits," in *Proc. Eur. Conf. Circuit Theory Design (ECCTD)*, Catania, Italy, Sep. 2017, doi: 10.1109/ECCTD.2017.8093225.

[18] T. Zaki *et al.*, "S-parameter characterization of submicrometer low-voltage organic thin-film transistors," *IEEE Electron Device Lett.*, vol. 34, no. 4, pp. 520–522, Apr. 2013, doi: 10.1109/LED.2013.2246759.

[19] M. Uno *et al.*, "Short-channel solution-processed organic semiconductor transistors and their application in high-speed organic complementary circuits and organic rectifiers," *Adv. Electron. Mater.*, vol. 1, no. 12, Dec. 2015, Art. no. 1500178, doi: 10.1002/aelm.201500178.

[20] K. Kotani, A. Sasaki, and T. Ito, "High-efficiency differential-drive CMOS rectifier for UHF RFIDs," *IEEE J. Solid-State Circuits*, vol. 44, no. 11, pp. 3011–3018, Nov. 2009, doi: 10.1109/JSSC.2009.2028955.

[21] R. Rotzoll *et al.*, "Radio frequency rectifiers based on organic thin-film transistors," *Appl. Phys. Lett.*, vol. 88, no. 12, Mar. 2006, Art. no. 123502, doi: 10.1063/1.2186384.

[22] S. Mandal and R. Sarpeshkar, "Low-power CMOS rectifier design for RFID applications," *IEEE Trans. Circuits Syst. I, Reg. Papers*, vol. 54, no. 6, pp. 1177–1188, Jun. 2007, doi: 10.1109/TCSI.2007.895229.

[23] P. Wei *et al.*, "High-efficiency differential RF front-end for a Gen2 RFID tag," *IEEE Trans. Circuits Syst. II, Exp. Briefs*, vol. 58, no. 4, pp. 189–194, Apr. 2011, doi: 10.1109/TCSII.2011.2124530.

[24] P. S. Heljo, M. Li, K. E. Lilja, H. S. Majumdar, and D. Lupo, "Printed half-wave and full-wave rectifier circuits based on organic diodes," *IEEE Trans. Electron Devices*, vol. 60, no. 2, pp. 870–874, Feb. 2013, doi: 10.1109/TED.2012.2233741.

[25] D.-H. Lee, J.-M. Kim, J.-W. Lee, and Y.-S. Kim, "Improved organic rectifier using polymethyl-methacrylate-poly 4-vinylphenol double layer," *Micro Nano Lett.*, vol. 6, no. 7, pp. 567–570, 2011, doi: 10.1049/mnl.2011.0094.

[26] C.-M. Kang, J. Roh, H. Shin, C. Lee, and H. Lee, "Investigation of improved performance for organic rectifying diodes via electrical annealing," *IEEE Access*, vol. 7, pp. 84082–84090, Jun. 2019, doi: 10.1109/ACCESS.2019.2924666.